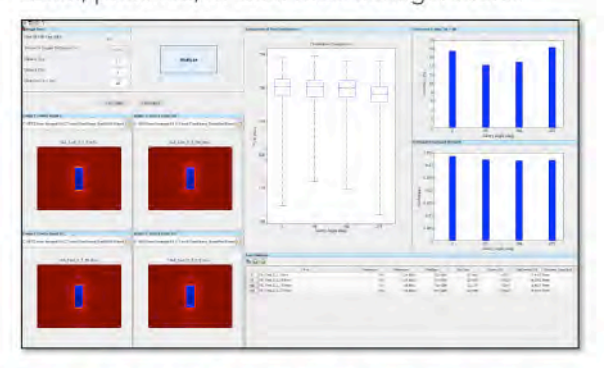


Varian Halcyon® RapidArc® & Picket Fence Analysis

By popular demand, RIT has extended our traditional RapidArc MLC analyses to support Varian Halcyon LINACs. In addition to the Millennium 120 and HD120 models, Halcyon users now have the option to perform fully automated RapidArc QA, with the flexibility to use distal, proximal, or dual MLC configurations.



New Routines & Workflow for Varian RapidArc® Tests

The new RapidArc Test 0.1 (dMLC Dosimetry) interface simultaneously loads and analyzes four cardinal gantry angle images and provides full automation for quick results. The software also features the new RapidArc Test 2 (Dose Rate and Gantry Speed) and Test 3 (Leaf Speed) routines for analyzing the various test modes against an open field image.

Enhanced MLC QA Automation Workflow



RapidArc Tests 0.2, 1.1, and 1.2, and the standard Picket Fence tests have been enhanced with (1) automated preprocessing for rotational and translation alignment, (2) expanded individual leaf analysis, and (3) support for a variety of common EPID sizes: 30x30, 30x40, 40x30, 40x40, and 43x43 cm.

Plan-Based Calibration for TomoTherapy® Registration

Utilize RIT's patented PBC technology to simplify your TomoTherapy Registration process for patient QA. A calibration file is no longer needed, scanner warm up is minimized, and variation in development time after exposure is no longer a significant factor. This saves you time and money, and potentially improves patient throughput.

Enhanced & Expanded Isocenter Optimization

RIT's popular 3D Winston-Lutz (Isocenter Optimization) routine now supports analysis on Elekta Unity machines. The updated interface will also display a range of 3 to 16 images within the same interface window. File names for exported results are automatically generated, saving users time. Choose to pass or fail on the Maximum Machine Deviation (R) or the Total Maximum Deviation (W), which includes the ball setup error.

EPID QA Phantom Couch Analysis

RIT software will analyze the EPID QA phantom when placed directly on the couch, providing an analysis closer to realistic patient positioning. The phantom's magnified dimensions are automatically calculated from the phantom size. This update provides physicists with more setup options when performing phantom analyses.



Expanded Phantom Analyses

RIT's Catphan Materials analysis will now analyze both horizontal slices and both vertical slices with ramps, in addition to an added measure of the yaw and tilt of the phantom, based on these ramps. Analyses for the QC-3 and QC-kV1 phantoms now feature a uniformity analysis.



CLICK TO EXPLORE THE NEW FEATURES IN DETAIL .

RADIMAGE.COM

RESEARCH ARTICLE

MEDICAL PHYSICS

Experimental and Monte Carlo-based determination of magnetic field correction factors $k_{B,Q}$ in high-energy photon fields for two ionization chambers

Mohamad Alissa^{1,2} | Klemens Zink^{1,2,3} | Ralf-Peter Kapsch⁴ Andreas A. Schoenfeld⁵ Stephan Frick⁴ Damian Czarnecki¹

Correspondence

Mohamad Alissa, Institute for Medical Physics and Radiation Protection, University of Applied Sciences Giessen, Giessen, Germany. Email: mohamad.alissa@lse.thm.de

Abstract

Background: The integration of magnetic resonance tomography into clinical linear accelerators provides high-contrast, real-time imaging during treatment and facilitates online-adaptive workflows in radiation therapy treatments. The associated magnetic field also bends the trajectories of charged particles via the Lorentz force, which may alter the dose distribution in a patient or a phantom and affects the dose response of dosimetry detectors.

Purpose: To perform an experimental and Monte Carlo-based determination of correction factors $k_{B,Q}$, which correct the response of ion chambers in the presence of external magnetic fields in high-energy photon fields.

Methods: The response variation of two different types of ion chambers (Sun Nuclear SNC125c and SNC600c) in strong external magnetic fields was investigated experimentally and by Monte Carlo simulations. The experimental data were acquired at the German National Metrology Institute, PTB, using a clinical linear accelerator with a nominal photon energy of 6 MV and an external electromagnet capable of generating magnetic flux densities of up to 1.5 T in opposite directions. The Monte Carlo simulation geometries corresponded to the experimental setup and additionally to the reference conditions of IAEA TRS-398. For the latter, the Monte Carlo simulations were performed with two different photon spectra: the 6 MV spectrum of the linear accelerator used for the experimental data acquisition and a 7 MV spectrum of a commercial MRI-linear accelerator. In each simulation geometry, three different orientations of the external magnetic field, the beam direction and the chamber orientation were investigated.

Results: Good agreement was achieved between Monte Carlo simulations and measurements with the SNC125c and SNC600c ionization chambers, with a mean deviation of 0.3% and 0.6%, respectively. The magnitude of the correction factor $k_{B,Q}$ strongly depends on the chamber volume and on the orientation of the chamber axis relative to the external magnetic field and the beam directions. It is greater for the SNC600c chamber with a volume of 0.6 cm³ than for the SNC125c chamber with a volume of 0.1 cm³. When the magnetic field direction and the chamber axis coincide, and they are perpendicular to the beam direction, the ion chambers exhibit a calculated overresponse of less than 0.7(6)% (SNC600c) and 0.3(4)% (SNC125c) at 1.5 T and less than 0.3(0)% (SNC600c) and 0.1(3)% (SNC125c) for 0.35 T for nominal beam energies of 6 MV and 7 MV. This chamber orientation should be preferred, as $k_{B,O}$ may increase significantly

This is an open access article under the terms of the Creative Commons Attribution License, which permits use, distribution and reproduction in any medium, provided the original work is properly cited.

© 2023 The Authors. Medical Physics published by Wiley Periodicals LLC on behalf of American Association of Physicists in Medicine.

¹Institute for Medical Physics and Radiation Protection, University of Applied Sciences Giessen, Giessen, Germany

²Department of Radiotherapy and Radiation Oncology, University Medical Center Giessen and Marburg, Marburg, Germany

³Marburg Ionbeam Therapy Center (MIT), Marburg, Germany

⁴German National Metrology Institute (PTB), Braunschweig, Germany

⁵Sun Nuclear, A Mirion Medical Company, Melbourne, Florida, USA

in other chamber orientations. Due to the special geometry of the guard ring, no dead-volume effects have been observed in any orientation studied. The results show an intra-type variation of 0.17% and 0.07% standard uncertainty (k=1) for the SNC125c and SNC600c, respectively.

Conclusion: Magnetic field correction factors $k_{B,O}$ for two different ion chambers and for typical clinical photon beam qualities were presented and compared with the few data existing in the literature. The correction factors may be applied in clinical reference dosimetry for existing MRI-linear accelerators.

KEYWORDS

Dosimetry, magnetic fields, magnetic field correction factors, Monte Carlo, MR-linac

INTRODUCTION

The integration of magnetic resonance tomography into clinical linear accelerators (linacs) provides highcontrast, real-time imaging during treatment which may help to reduce dose to healthy tissue, and facilitates online-adaptive workflows in radiation therapy treatments. However, the strong magnetic field of the MRI impacts the trajectories of the charged particles set in motion by the high-energy photons. Due to the Lorentz force, the trajectories become spiral and the dose distribution, as well as the dose response of applied radiation detectors, may change. 1-3 The effect of magnetic fields on the response of ionization chambers has been investigated thoroughly in experimental and Monte Carlo studies on several chamber designs.4-11 Its magnitude depends on chamber characteristics, such as the (effective) sensitive volume and material composition, but also on the magnetic field strength, the energy spectrum of the incident beam and the chamber orientation with respect to the magnetic field and beam directions. In most cases, large Farmer-type ion chambers were investigated under reference conditions. Meijsing et al.3 studied the response variation of the NE2571 ion chamber experimentally and with Monte Carlo simulations for different orientations and strengths of magnetic fields. They concluded that the response variation of the chamber is related to the number and length of electron trajectories entering the sensitive volume of a chamber. Spindeldreier et al.5 investigated the impact of the active volume on the magnetic field correction factor $k_{B,O}$ (as defined in section 2.1) by testing a series of PTW-30013 Farmer chambers with different chamber radii. They found a maximum increase in chamber response of 8.8% for the magnetic field strength of 1.1 T applied perpendicular to the incoming beam and the chamber axis. De Prez et al. 9 measured k_Q as well as $k_{B,Q}$ values for two Farmer-type chambers (PTW-30013 and IBA-FC65-G) on a pre-clinical 7 MV MRI-linac at 0 T and 1.5 T with a water calorimeter.

Recently, several studies discussed the effect of electrically shielded regions in the chamber cavity near the chamber stem. Some guard ring geometries span an electric field from the guard ring to the outer electrode

(chamber wall). Consequently, electrons released in this part of the chamber cavity will not be collected by the central electrode and will not contribute to the dosimeter reading M_Q . Malkov and Rogers et al. 10,11 investigated this so-called dead volume by approximating its geometry as a slice with thickness d located next to the guard ring. They calculated the chamber's response dependence on d for a wide range of ion chambers in external magnetic fields and found a good agreement between their Monte Carlo simulations and experimental data, if the thickness d of the dead volume was between 0.5 and 1 mm. Delfs et al.8 developed a more sophisticated model of the dead volume based on proton microbeam tomography of the effective sensitive volume, i.e. cavity volume minus dead volume, and finite element calculations of the chamber's electric field. By amending the Monte Carlo models of the respective chambers accordingly, the agreement between measurements and simulations was better than 1%. By neglecting the dead volume effect, however, differences of up to 6% were observed. Aside from investigating small thimble chambers under reference conditions, Delfs et al.8 performed measurements revealing that the SNC125c ionization chamber (Sun Nuclear, A Mirion Medical Company, Melbourne, FL) is not affected by dead volume.

24734090, 0, Downloaded from https://aapm.onlinelibrary.wiley.com/doi/10.1002/mp.16345 by Cochrane Germany, Wiley Online Library on [23.032023]. See the Terms and Conditions (https://onlinelibrary.wiley.com/terms-and-conditions) on Wiley Online Library for rules of use; OA articles are governed by the applicable Creative Commons Licenses

The aim of the present study is the determination of the magnetic correction factor $k_{B,O}$ for two commercially available thimble ionization chambers SNC125c and SNC600c (Sun Nuclear, A Mirion Medical Company. Melbourne, FL), which are in wide clinical use. To perform a complete characterization of these chambers, the response variation of the two ionization chambers for different magnetic fields strengths and magnetic field directions was studied experimentally and by Monte Carlo simulations. The measurements were performed at the German National Metrology Institute (PTB, Braunschweig, Germany). The Monte Carlo models of the ion chambers were created in a previous, joint study with the Canadian National Metrology Institute (NRC, Ottawa, Canada) on the determination of the beam quality correction factors $k_{\rm Q}$. Therein, the chamber models were cross-validated by independent Monte Carlo simulations and experimental data.

The magnetic field correction factor $k_{B,Q}$ was calculated for the x-ray spectrum of the Elekta Unity MR-linac (Elekta AB, Stockholm, Sweden), with a nominal energy of 7 MV bremsstrahlung, and also for the known 6 MV spectrum of the PTB linac to back up the Monte Carlo results with experimental data. The latter spectrum may serve as approximation of the 6 MV spectrum of ViewRay MR-linacs. Thus, the correction factors shown here can be used directly for clinical MR-linacs.

2 MATERIALS AND METHODS

Magnetic field correction factor $k_{B,Q}$

In the presence of strong magnetic fields \vec{B} the wellknown equation for the determination of dose-to-water D_w in clinical photon dosimetry, ^{13–15} i.e.

$$D_{w} = M_{\mathcal{Q}} \cdot N_{D,w,Q_{0}} \cdot k_{\mathcal{Q},Q_{0}} \tag{1}$$

has to be expanded by a new correction factor $k_{B,O}^9$:

$$D_{w}^{B} = M_{Q}^{B} \cdot N_{D,w,Q_{0}} \cdot k_{Q,Q_{0}} \cdot k_{B,Q}$$
 (2)

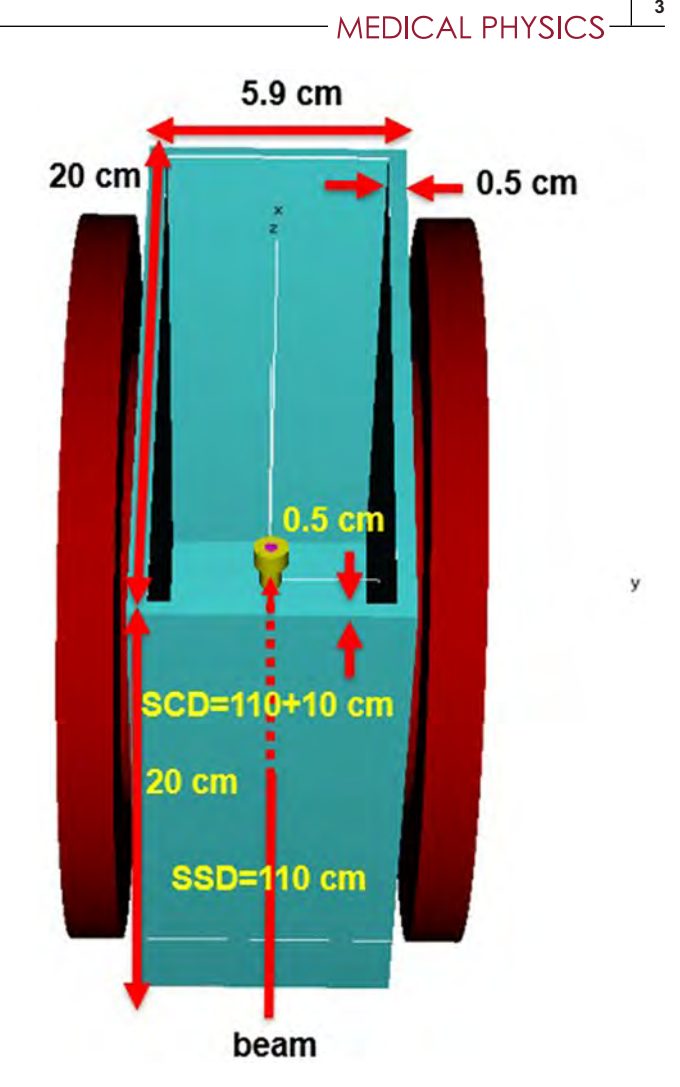
Herein M_Q^B and M_Q are the corrected dosimeter readings at beam quality Q with and without a magnetic field \vec{B} , N_{D,w,Q_0} is the absorbed dose-to-water calibration coefficient at reference beam quality Q_0 . Furthermore, k_{Q,Q_0} is the beam quality correction factor taking into account the different response of the ion chamber in the beam quality Q with respect to the reference beam quality Q_0 . $k_{B,O}$ is the correction factor correcting the different ion chamber response due to the presence of the external magnetic field. From equations (1) and (2) it follows, that for a given beam quality $Q, k_{B,Q}$ is given as⁴

$$k_{B,Q} = \frac{D_{w,Q}^B}{D_{w,Q}} \cdot \frac{M_Q}{M_Q^B} = \frac{D_{w,Q}^B}{D_{w,Q}} \cdot \frac{\overline{D}_{det,Q}}{\overline{D}_{det,Q}^B}$$
(3)

To calculate $k_{B,Q}$ with Monte Carlo simulations, the measured charges M_Q and M_Q^B in equation (3) were replaced by the scored dose per incident fluence on the phantom $\overline{D}_{det,Q}$ and $\overline{D}_{det,Q}^{D}$ in the air filled cavity of the ion chamber model without and with an external magnetic field Ŕ.

2.2 **Experimental setup**

The measurements were performed at the German National Metrology Institute (PTB). The facility has coupled an electromagnet (Type ER 073W, Bruker BioSpin GmbH) with an Elekta Precise linac operating at 6 MV nominal photon energy. The electromagnet can generate magnetic flux densities of up to 1.5 T



The Monte Carlo model of the experimental setup at PTB, which was used for the Monte Carlo calculations of the chamber response given in Figure 4. A longer water phantom was used for the measurements of the SNC600c chamber in orientation c (see Figure 2), which measured 28 cm instead of 20 cm in beam direction.

in opposite directions between its pole shoes, where a small water phantom sized $20 \times 20 \times 5.9 \text{ cm}^3$ or $28 \times 20 \times 5.9$ cm³ was installed (see Figure 1). Two different types of ion chambers were investigated: the farmer-type chamber SNC600c (Sun Nuclear, A Mirion Medical Company, Melbourne, FL) and the small thimble chamber SNC125c (also Sun Nuclear). The SNC600c has a sensitive volume of 0.6 cm³, and the chamber wall is made of resin impregnated graphite. The SNC125c has a sensitive volume of 0.1 cm³ and the wall is made of high purity graphite. More information about the chambers is given in Figure 3 and Table 4. The chambers were placed in the water phantom at a depth of 10 g/cm². The field size at this water depth was 4x10 cm². Due to the special geometry of the electromagnet, the source-surface distance (SSD) and the source-chamber distance (SCD) differ slightly from the reference conditions given in the TRS-398 code-of-practice (CoP) (see Table 2).

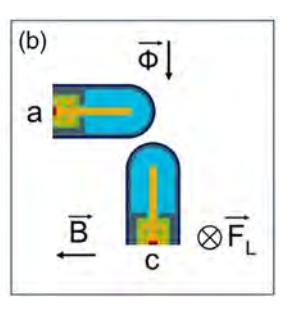


FIGURE 2 Orientations of the ion chambers relative to the magnetic field \vec{B} and the photon beam direction $\vec{\phi}$. The orientation (a) is not experimentally possible due to geometry constraints of the pole faces . The direction of the Lorentz force \vec{F}_L is given for B_x and (negatively charged) electrons as described by de Pooter et al. 16.

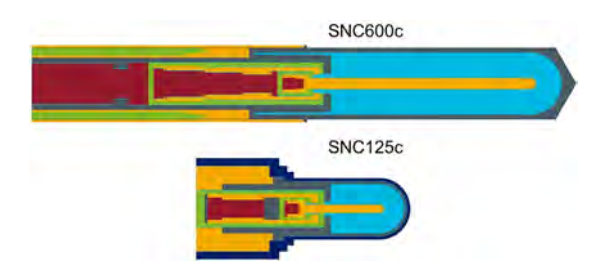


FIGURE 3 Cross sections of the Monte Carlo models of the investigated ion chambers. Both chamber drawings have a different scaling. Different colors represent different materials. The chamber models were validated in.¹².

TABLE 1 Twelve ionization chambers from different production batches used in this work.

Ionization	Production	Batch	N _{D,w,Q0} in
chamber	date	number	10' Gy/C
SNC125c	April 2020	256353	27.65
	April 2020	256353	27.75
	April 2021	266541	28.49
	April 2022	270233	28.21
	April 2022	270429	28.47
	June 2022	271015	28.36
SNC600c	January 2021	265733	5.163
	January 2021	265733	5.158
	January 2021	265733	5.160
	May 2022	270587	5.165
	August 2022	271546	5.091
	September 2022	271903	5.178

TABLE 2 The geometrical reference conditions according to IAEA TRS-398 code of practice and the geometrical measurement conditions as used in the experimental setup at PTB.

SET-UP	TRS-398	РТВ
Source to surface distance (SSD)	90 cm	110 cm
Source to chamber distance (SCD)	100 cm	120 cm
Measurement depths	10 g/cm ²	10 g/cm ²
Field size at (SSD)	$10 \times 10 \text{ cm}^2$	$4 \times 10 \text{ cm}^2$

The experimental setup puts the magnetic field direction always perpendicular to the incident photon beam. For this reason, in the Monte Carlo set up, the beam axis was oriented along the z-axis and the magnetic field along the x-axis (see Figure 1). It should be noted that the magnetic field has only a component in the x-direction. In the following the x component of the magnetic field will be used to describe the magnetic field, where a negative sign indicates an opposing direction of the magnetic field vector. This setup results in two possible ion chamber orientations relative to the beam and to the magnetic field. A third orientation with the ion chamber axis being parallel to the magnetic field could be realized in the Monte Carlo model, but not in the experimental setup. The three orientations are given in Figure 2a and are defined as (a), (c) and (d) according to de Pooter et al. 16 In orientation (d), the average Lorentz force is parallel to the chamber axis, i.e. the secondary electrons will drift towards the tip of the chamber or towards the stem. In that case, it may be expected that the response of the chamber as a function of the magnetic field strength is non-symmetric about B = 0 T. In orientations (a) and (c), the Lorentz force drives the electrons towards the lateral chamber wall, and consequentially, the chamber response as a function of \vec{B} should be symmetrical about $\vec{B} = 0$ T. The difference between orientations (a) and (c) is that in orientation (a) the beam is perpendicular to the chamber axis, while in orientation (c) the beam and the chamber axis are parallel to each other. All measurements were performed in a water phantom of 20x20x5.9 cm³ (Figure 1), except those with the SNC600c in orientation (c). Because of the rigid chamber stem of the SNC600c, it was placed in a longer water phantom with a length of 28 cm instead of 20 cm in beam direction. The downstream elongation of the phantom had no impact on the results, as was examined in preliminary measurements and Monte Carlo simulations. Six ionization chambers of the type SNC600c and six ionization chambers of the type SNC125c, as listed in Table 1, were investigated in this study. To quantify the reproducibility of the chamber positioning in the experimental setup, measurements with one SNC125c chamber were repeated three times on three different days.

Monte Carlo simulations 2.3

All Monte Carlo calculations were performed with the EGSnrc code system (version 2020).¹⁷ The simulation parameters are summarized in Table 3. In this study the less efficient emf macros.mortran was used for particle simulation in the external magnetic field. It should be noted that an improved macro eemf macros.mortran is already available in the current EGSnrc installation. However, it could already be shown in a previous study by means of Fano-test that with the older macro a

TABLE 3 Summary of simulation properties and parameters used for the Monte Carlo simulations.

Item	Description	References
Code	EGSnrc code system,	Kawrakow et al. ¹⁷
	egs++ library,	Kawrakow et al. ²²
	egs_chamber	Wulff et al. ²³
	emf macros.mortran	Bielajew ²⁴
Validation	Fano cavity test	Results in Appendix
Timing	Absorbed dose to water $D_{\rm W}$ in the sensitive volume of the chamber for photon spectra with B field took 150 and 280 single CPU hours (2.1 GHz), for the SNC600c and SNC125c ionization chambers, respectively.	
Source description	Collimated isotropic point sources with 7 MV (TPR20,10 = 0.691) and 6 MV photon spectrum (TPR20,10 = 0.677)	Ahmad et al. ²¹
Cross-sections	XCOM photon cross section with multiconfiguration DiracFock renormalization factor for the photoelectric effect (mcdf-xcom)	
Transport parameters	Boundary crossing algorithm: Exact; transport and particle production threshold energy of 512 keV for electrons and 1 keV for photons.	
Variance reduction techniques	Intermediate phase space storage (IPSS); Photon cross-section enhancement (XCSE) volume with an XCSE factor of 128 and Russian Roulette range rejection technique with a survival probability of 1/128.	Wulff et al. ²³
Scored quantities	Absorbed dose to water and dose to air	
Statistical uncertainties	≤ 0.1% for all calculated quantities	
Statistical method	History-by-history	
Postprocessing	None	

Summary of the materials and geometric data of the ionization chambers.

lonization chamber	Material	Wall Thickness	Central electrode Material	Radius	Sensitive volume Material	Radius	Length
SNC125c	Graphite	0.25 mm	Al	0.4 mm	Air	2.375 mm	7.05 mm
	PMMA	0.30 mm					
	Paint	0.05 mm					
SNC600c	Graphite	0.43 mm	Al	0.55 mm	Air	3.05 mm	22.7 mm
	Paint	0.05 mm					

comparable accuracy of the radiation transport can be achieved, albeit with higher computing time. 18 The ICRU Report 90¹⁹ recommendations were followed with regards to the ionization energies I and the density correction δ . Radiation sources were simulated as collimated isotropic point sources with a 6 MV or a 7 MV photon spectrum. The 6 MV spectrum was extracted from a complete BEAM simulation of the Elekta Precise linac at PTB Braunschweig and may also be used to represent the ViewRay machine,²⁰ the 7 MV spectrum was taken from Ahmad²¹ and represents the spectrum of the commercially available Elekta Unity MR-linac.

The two ion chamber types SNC600c and SNC125c were modelled with the C++ class library egspp²² based on technical drawings provided by the manufacturer. The cross sections of the chamber models are displayed in Figure 3, further chamber details are sum-

marized in Table 4. One distinct feature of both chambers is the geometry of the guard electrode: it is flat over the entire base area of the air-filled volume. Therefore. both chambers should show no dead-volume effects. In the present study, two series of Monte Carlo simulations were performed: (a) PTB setup: this geometry corresponds to the experimental setup at PTB. It includes the pole shoes and the PMMA water phantom (see Figure 1 and Table 2). For this geometry, the variation of the dose ratio $\overline{D}_{det,O}^{\prime}/\overline{D}_{det,O}$ as a function of the external magnetic field B was calculated using the 6 MV spectrum of the PTB linac, which was already used in previous studies²⁰; (b) TRS-398 setup: this setup corresponds to the TRS-398 reference conditions¹³ (see Table 2) with water phantom dimension of 30x30x30 cm³. Preliminary simulations of the dose ratio $\overline{D}_{det,Q}^B/\overline{D}_{det,Q}$ in

same ionization chambers showed that the measurement setup uncertainty was within 0.15%. The results of measurements with 6 different ionization chambers per chamber model show an intra-type variation of 0.17% and 0.07% standard uncertainty (k=1) for the SNC125c and SNC600c, respectively. The results are consistent with those published by Woodings et al.,23 who investigated the k_{BO} values and intra-type variations of Farmer type ionization chambers PTW30013 and FC65-G in external magnetic fields.

both setups showed that the effects of the different field and phantom sizes, as well as the slightly different setup distances on the calculated dose ratios were negligible (< 0.1%). All dose quantities for the determination of the magnetic field correction factor $k_{B,O}$, given in eq. (3), were calculated in the TRS-398 setup. To calculate the dose to water $D_{w,Q}^{B}$ and $D_{w,Q}$, a small water disc with radius 0.1 mm and height 0.1 mm was positioned symmetrically around the point of measurement at depth $z_0 = 10$ cm. The dose to the ion chamber $\overline{D}_{det,Q}$ and $\overline{D}_{det,O}^{\nu}$ was calculated within the active volume of each chamber, where the chambers' reference points were at z_0 . The correction factors $k_{B,Q}$ were calculated for both

The asymmetry of the data plot around B = 0 T for chamber orientation (d) is strongly pronounced for the smaller SNC125c chamber (Figure 4a) and has a maximum value of about 2% at $B_x = 0.8$ T. Note that in orientation (d) \vec{F}_{l} is parallel to the chamber axis. This orientation shows good agreement between the Monte Carlo simulations and measurement data. All in all, the agreement of all measured and Monte Carlo based values for all B-field strengths is within 0.5% for this chamber model in this orientation. The deviation in the dose ratios seen for the chambers may be due to geometrical or material tolerances in the production process.

Dead volume effects 2.3.1

photon spectra according to eq. (3).

For the large chamber SNC600c in orientation (d), the asymmetry between positive and negative B-field values is well below 0.5%. The asymmetry is slightly more pronounced in the measurement data than in the Monte Carlo data leading to deviations of about 1% between measurement and simulation for negative B-fields. The reasons for this deviation are not quite clear, but one assumption is that there are still small differences in the geometry or material composition of the Monte Carlo model and the real ion chambers. The agreement of the experimental results between all chambers is excellent, i.e. within 0.16%, meaning that the specimen scatter for the SNC600c ion chambers is very small. In orientation (c) with magnetic field perpendicular to the chamber axis

Similar to the studies from Malkov and Rogers. 10,11 the hypothetical dead volume was modeled as a slice of thickness d just above the guard ring of the cylindrical chambers SNC125c and SNC600c. For the thickness d values of 0.1, 0.2 and 0.3 mm for the small SNC125c chamber and 0.3, 0.5 and 0.7 mm for the large SNC600c chamber were applied, i.e. the dose was scored in the active volume given in Figure 3 minus the slice of thickness d. The simple dead volume model from Malkov and Rogers seems to be adequate for the SNC chambers, since the guard ring is flat and fills the entire diameter of the chamber. Delfs et al.8 already investigated the SNC125c chamber and found that this form of guard ring does not produce a dead-volume. As the large SNC600c chamber has a very similar geometry, it was assumed that the simple model for the dead volume geometry is sufficient for the purpose of this study.

> and the beam parallel to its axis, the ratio $\overline{D}_{det O}/\overline{D}_{det O}$ is symmetrical around B = 0 T, since the Lorentz force drives the electrons towards the lateral chamber wall and the geometry is symmetrical with respect to the magnetic field direction. The variation of the dose ratio is largest in this chamber orientation and reaches up to 8.5% for the SNC600c. Equivalent to Figure 4b, the experimental data for the different chambers are in nearly perfect agreement. For larger B-values there is an increasing deviation between Monte Carlo based and experimental data; the deviation is in the range of 1%. For the small chamber SNC125c and orientation (c), the variation of the dose ratio with the magnetic field strength is only in the range of 4%. Regarding the experimental data, Figure 4c clearly shows a deviation of the dose ratios for increasing B-values between the chambers.

RESULTS AND DISCUSSIONS

This is in accordance with the results given in Figure 4a.

3.1 Chamber response as a function of

Figure 4 presents the ratio $\overline{D}_{det,Q}^B/\overline{D}_{det,Q}$ of the investigated chambers as a function of the magnetic field strength B for the three chamber orientations shown in Figure 2 and for the 6 MV photon spectrum. Therein, the left column shows the results for the SNC125c and the right column shows those for the SNC600c, Each row corresponds to one of the three chamber orientations with respect to the magnetic field \vec{B} and the beam directions. The Monte Carlo results shown in this figure were calculated in the PTB setup, but as mentioned above, the different setups had no significant impact on the calculated dose ratios. Repeated measurements with the

and-conditions) on Wiley Online Library for rules of use; OA articles are governed by the applicable Creative Commons License

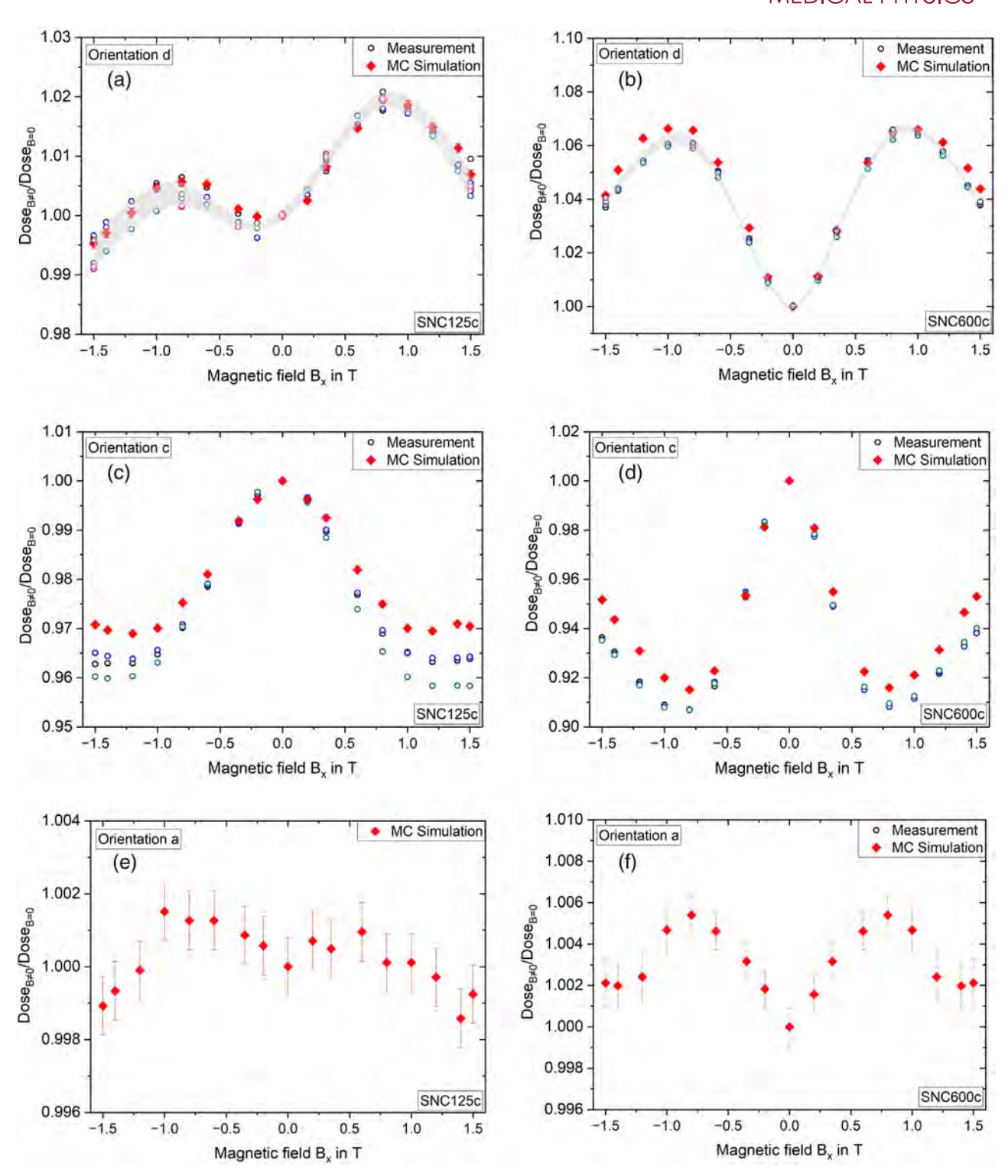


FIGURE 4 Comparison of experimental and Monte Carlo based results of the ratio $\overline{D}_{det,Q}^B/\overline{D}_{det,Q}$ as a function of the magnetic field B for the ion chambers SNC125c (left column) and SNC600c (right column) for 6 MV photons. Measured values for the chambers are represented by open circles. Each measurement series with an individual ionization chamber is represented by a different symbol color. Panels (a) and (b) each show the 1σ -standard deviation of six different ionization chambers as gray area, indicating the intra-type variation for the SNC125c and SNC600c respectively. The uncertainty bars in case of the Monte Carlo data represent the type-A-uncertainties, in case of the experimental data the standard deviation of the mean value of ten electrometer readings (1σ). Note the different scales of the y-axes.

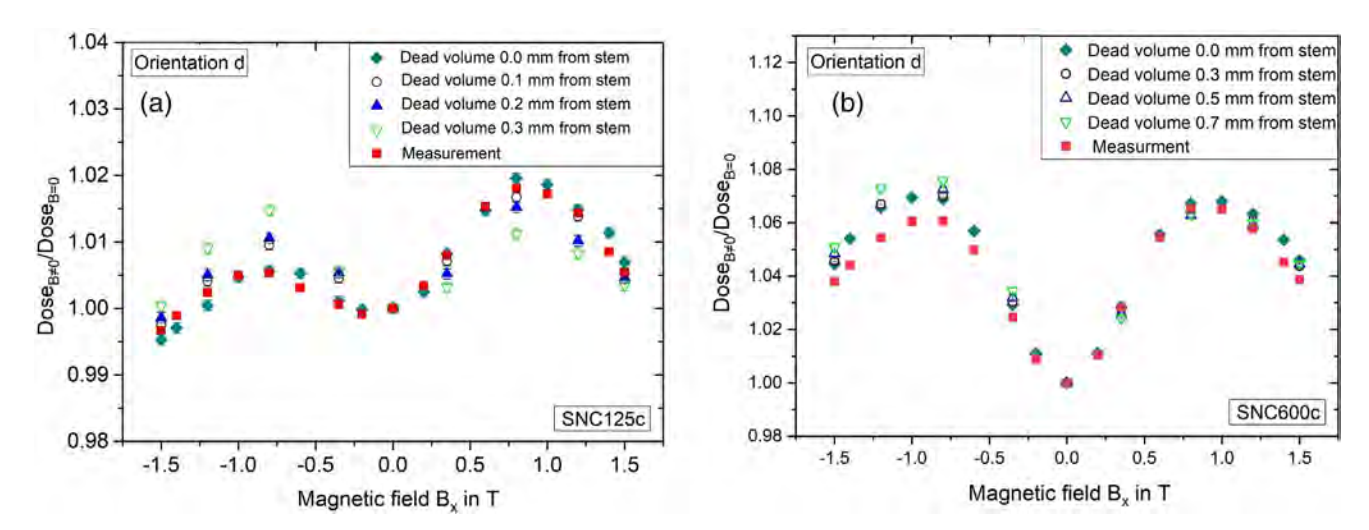


FIGURE 5 Dose ratio $\overline{D}_{det,Q}^{B}/\overline{D}_{det,Q}$ as a function of the magnetic field strength for the SNC125c and SNC600c chamber with differently sized dead volumes for the 6 MV spectrum. The dead volumes were modelled as thin slices of given thickness next to the guard ring. Note that the slice thicknesses chosen for the SNC600c were larger than those used for the SNC125c, due to its larger chamber cavity.

With increasing absolute *B*-values there are also increasing deviations between the Monte Carlo and the experimental data. These deviations are in the range of 1% for *B*-values of 1.5 T in opposite directions. This indicates that there are differences in the geometry of the Monte Carlo model and the real ion chamber. However, one has to keep in mind that chamber orientations (c) and (d), where the magnetic field is perpendicular to the chamber axis, should not be used in clinical routine, since the magnetic field effects are maximized and otherwise insignificant chamber-to-chamber variation can become apparent. Instead, orientation (a) (Figure 4e &

f) should be used, where $\overline{D}_{det,Q}/\overline{D}_{det,Q}$ is near unity. The deviation from unity is less than 0.6% for the SNC600c and less than 0.2% for the SNC125c at all magnetic field strengths. Therefore, this orientation appears as the optimal direction for clinical dosimetry. For both chambers, the Monte Carlo data show a small asymmetry around B=0 T. Due to the small dimensions of the water phantom between the pole shoes of the electromagnet, unfortunately, no measurement data could be acquired in this orientation.

3.1.1 | Effect of a dead volume

Figure 5 shows the potential effect of dead volume on the dose ratios $\overline{D}_{det,Q}^B/\overline{D}_{det,Q}$ for both chambers. The best agreement between measurement and Monte Carlo simulation results in a zero dead volume for both chambers. This is in agreement with the findings of Delfs, who examined the effective sensitive volume of the SNC125c chamber with proton microbeam scans and concluded that it has no dead volume. According to our measurements and Monte Carlo simulations, this

is also true for the SNC600c chamber. This result is expected, since the geometry of the SNC600c's guard is very similar to that of the SNC125c. In orientation (a) the effect of dead volume does not play a role since the Lorenz force will not deflect electrons toward or against the stem.

3.2 \mid Magnetic field correction factor $k_{B,O}$

The magnetic field correction factor $k_{B,Q}$ was calculated according to equation (3) using the TRS-398 setup described in section 2.3, i.e. a 30x30x30 cm³ water phantom, a field size of 10x10 cm² and the setup distances summarized in Table 2. The dose ratios $\overline{D}_{det,Q}^B/\overline{D}_{det,Q}$ shown in Figure 4 were also recalculated in this geometry, but the ratios do not differ by more than 0.1% from those calculated in the PTB setup. The factors $k_{B,Q}$ of both ion chambers, all chamber orientations and both photon spectra are presented in Figure 6 as a function of the magnetic field B and compared to available data from literature.⁸

The magnitude of $k_{B,Q}$ strongly depends on the chamber volume, i.e. is greater for the SNC600c chamber than for the SNC125c chamber. It also depends on the orientation of the chamber relative to magnetic field and beam directions. For orientation (c) both chambers show an under-response for magnetic fields $B \neq 0$, i.e. $k_{B,Q} > 1$. For the SNC600c chamber the under-response is up to 9% for a magnetic field $B_x \approx 0.8$ T. For the smaller SNC125c chamber it is about 3% for $B_x \approx 1.0$ T. As the Lorentz force in this orientation drives the electrons towards the chamber wall (see Figure 2), the resulting correction factor $k_{B,Q}$ is symmetrical about B = 0 T. The impact of the different photon spectra used here (6 MV

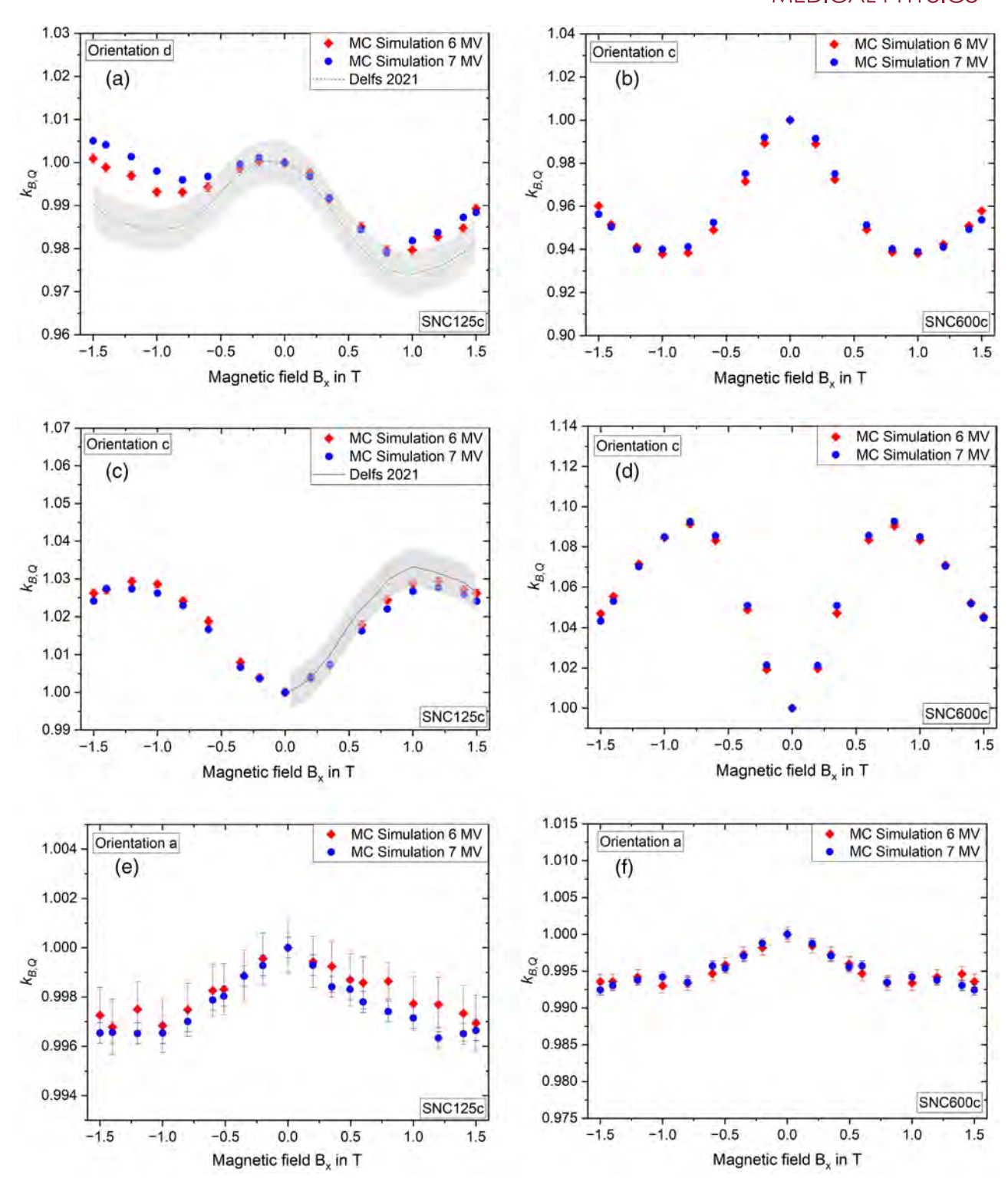


FIGURE 6 Magnetic field correction factors $k_{B,Q}$ of the ion chambers SNC125c and SNC600c as a function of the magnetic field strength *B* for different chamber orientations with respect to the magnetic field and beam directions (see Figure 2). Two different photon spectra were applied: the 6 MV spectrum of the PTB-linac²⁰ and the 7 MV spectrum of the Elekta Unity MR-linac.²¹ The type-A standard uncertainty is given by the uncertainty bars or by the symbol width. The data from Delfs et al.⁸ were calculated with a 6 MV linac spectrum in a geometry that closely resembles the PTB setup of the present study. The uncertainty of Delf's values is given by the shaded area. Note the different scales of the y-axes.

TABLE 5 Magnetic field correction factors for existing MRI-linear accelerators for ionization chambers SNC125c and SNC600c for orientation (a). The differences between $k_{B,Q}$ values for opposing magnetic field directions are within the statistical uncertainty.

		Source	Source
lonization chamber	<i>B</i> field	6 MV <i>k_{B,Q}</i>	7 MV <i>k_{B,Q}</i>
SNC125c	$B_{\rm x} = \pm 0.35 {\rm T}$	0.999(0)	0.998(7)
	$B_x = \pm 0.5 \text{ T}$	0.998(6)	0.998(2)
	$B_x = \pm 1.5 \text{ T}$	0.997(1)	0.996(5)
SNC600c	$B_x = \pm 0.35 \text{ T}$	0.997(0)	0.997(0)
	$B_x = \pm 0.5 \text{ T}$	0.995(4)	0.995(2)
	$B_x = \pm 1.5 \text{ T}$	0.993(1)	0.992(4)

and 7 MV) is below 0.2% for both chambers and all B-values. The Monte Carlo based $k_{B,Q}$ data from Delfs et al.⁸ agree within one standard uncertainty with the results of this study, as can be seen in Figure 6c, while for orientation (d) the agreement is within 1%-1.5% (see Figure 6a).

An asymmetry of $k_{B,Q}$ around B=0 T is clearly visible when the SNC125c chamber is positioned in orientation (d). The variation of the correction factor for B-values between ± 1.5 T is in the range of 2%. An influence of the photon energy is visible only for negative B fields and amounts to no more than 0.5% for B_x =-1.5 T. Delfs et al. also produced $k_{B,Q}$ data for a 6 MV spectrum, which agree with the results of this study to within 1% for all magnetic field strengths.

The correction factor $k_{B,Q}$ and its variation with the external B–field is smallest in chamber orientation (a), which is the preferred orientation for clinical use. For the SNC125c chamber, the largest deviation from unity is 0.4% at magnetic field strengths near $B_x = 1.5$ T. Even for the larger SNC600c chamber, the deviation from unity is less than 1.2% over the whole range of investigated \vec{B} -values. In both cases, the deviation from unity increases with increasing magnetic field strength. While the $k_{B,Q}$ values corresponding to the SNC125c are nearly the same for both energy spectra, they differ in the range of 0.5% for the larger SNC600c chamber. Table 5 summarizes the magnetic field correction factors $k_{B,Q}$ for commercially available MRI-linacs.

4 | CONCLUSION

The objective of the present study was the dosimetric investigation of the SNC125c and SNC600c ionization chambers in external magnetic fields. Together with the data from a previous study, in which the beam quality correction factors $k_{\rm Q}$ was determined for high-energy photon fields, the dosimetric behavior of these chambers is comprehensively characterized and the correction fac-

tors are available to the users for application in clinical routine with minimized dosimetric uncertainties.

The good agreement of experimental data and Monte Carlo simulations validated the applicability of the EGSnrc code system for radiation transport simulations in external magnetic fields. The results clearly showed that the magnetic field correction factor $k_{B,Q}$ strongly depends on the chamber volume and the chamber orientation with respect to the beam and magnetic field directions. The smallest deviation of $k_{B,Q}$ from unity occurs in case when the magnetic field is directed parallel to the chamber axis. $^{3,5,11,24-26}$ In that case, the correction factor is below 1.2% for the 0.6 cm³ SNC600c and below 0.4% for the small SNC125c chamber, even for a ^{2}B -field strength of 1.5 T, which is the maximum magnetic field strength of commercially available MRI-linacs.

Furthermore, a change in the dose response was confirmed when a dead volume was introduced to the ionization chamber model, the magnitude of which depends on the size and shape of the dead volume. As the effect of the magnetic field is significantly reduced in orientation (a), the effect of the dead volume may likewise be reduced in that orientation. Still, the simulation of the magnetic field correction factor $k_{B,Q}$ is challenging if an ionization chamber is affected, as prior research has demonstrated. The comparison of the simulated data with measurement data indicated that the investigated ionization chambers do not have a dead volume within the ionization chamber's air cavity. As a result, ionization chambers without a dead volume, like the SNC125c and SNC600c, may be modeled particularly well in Monte Carlo simulations.

ACKNOWLEDGMENTS

The authors have nothing to report.

Open access funding enabled and organized by Projekt DEAL.

CONFLICTS OF INTEREST STATEMENT

The authors declare no conflicts of interest.

REFERENCES

- Raaijmakers AJ, Raaymakers BW, Lagendijk JJ. Integrating a MRI scanner with a 6 MV radiotherapy accelerator: dose increase at tissue—air interfaces in a lateral magnetic field due to returning electrons. *Phys Med Biol.* 2005;50(7):1363.
- Raaijmakers AJ, Raaymakers BW, Lagendijk JJ. Magneticfield-induced dose effects in MR-guided radiotherapy systems: dependence on the magnetic field strength. *Phys Med Biol*. 2008;53(4):909.
- Meijsing I, Raaymakers B, Raaijmakers A, et al. Dosimetry for the MRI accelerator: the impact of a magnetic field on the response of a Farmer NE2571 ionization chamber. *Phys Med Biol*. 2009;54(10):2993.
- O'Brien DJ, Roberts DA, Ibbott GS, Sawakuchi GO. Reference dosimetry in magnetic fields: formalism and ionization chamber correction factors. *Med Phys.* 2016;43(8Part1):4915-4927.

24734090, 0, Downloaded from https://aapm.onlinelibrary.wiley.com/doi/10.1002/mp.16345 by Cochrane Germany, Wiley Online Library on [23:03/2023]. See the Terms and Conditions (https://onlinelibary.wiley.com/rems-and-conditions) on Wiley Online Library for rules of use; OA articles are governed by the applicable Creative Commons License

- Spindeldreier C, Schrenk O, Bakenecker A, et al. Radiation dosimetry in magnetic fields with Farmer-type ionization chambers: determination of magnetic field correction factors for different magnetic field strengths and field orientations. *Phys Med Biol.* 2017;62(16):6708.
- Pojtinger S, Dohm OS, Kapsch RP, Thorwarth D. Ionization chamber correction factors for MR-linacs. *Phys Med Biol.* 2018;63(11):11NT03.
- Reynolds M, Fallone B, Rathee S. Dose response of selected ion chambers in applied homogeneous transverse and longitudinal magnetic fields. *Med Phys.* 2013;40(4):042102.
- 8. Delfs B, Blum I, Tekin T, et al. The role of the construction and sensitive volume of compact ionization chambers on the magnetic field-dependent dose response. *Med Phys.* 2021;48(8):4572-4585.
- Prez Ld, Woodings S, Pooter Jd, et al. Direct measurement of ion chamber correction factors, k_Q and k_B, in a 7 MV MRI-linac. *Phys Med Biol*. 2019;64(10):105025.
- Malkov VN, Rogers D. Sensitive volume effects on Monte Carlo calculated ion chamber response in magnetic fields. *Med Phys.* 2017;44(9):4854-4858.
- Malkov VN, Rogers D. Monte Carlo study of ionization chamber magnetic field correction factors as a function of angle and beam quality. Med Phys. 2018;45(2):908-925.
- Alissa M, Zink K, Tessier F, Schoenfeld AA, Czarnecki D. Monte carlo calculated beam quality correction factors for two cylindrical ionization chambers in photon beams. *Phys Med*. 2022;94: 17-23.
- Absorbed Dose Determination in External Beam Radiotherapy, no. TRS-398 in Technical Reports Series. International Atomic Energy Agency - IAEA, Vienna, 2001.
- Almond PR, Biggs PJ, Coursey BM, et al. AAPM's TG-51 protocol for clinical reference dosimetry of high-energy photon and electron beams. *Med Phys.* 1999;26(9):1847-1870.
- DIN 6800-2, Procedures of dosimetry with probe-type detectors for photon and electron radiation - Part 2: Ionization chamber dosimetry of high energy photon and electron radiation, DIN -Normenausschuss Radiologie (NAR), 2020.
- de Pooter J, Billas I, de Prez L, et al. Reference dosimetry in mrilinacs: evaluation of available protocols and data to establish a code of practice. *Phys Med Biol.* 2021;66(5):05TR02.
- Kawrakow I, Mainegra-Hing E, Rogers DWO, Tessier F, Walters BRB. The EGSnrc Code System: Monte Carlo Simulation of Electron and Photon Transport, 2021. https://doi.org/10.4224/ 40001303
- Alissa M, Zink K, Czarnecki D. Investigation of monte carlo simulations of the electron transport in external magnetic fields using fano cavity test, Zeitschrift fuer Medizinische Physik, (2022). https://doi.org/10.1016/j.zemedi.2022.07.002
- Seltzer SM, Fernandez-Varea JM, Andreo P, et al. Report 90: Key data for ionizing-radiation dosimetry: Measurement standards and applications. J ICRU. 2014;14(1):1742-3422.
- Tikkanen J, Zink K, Pimpinella M, et al. Calculated beam quality correction factors for ionization chambers in MV photon beams. *Phys Med Biol.* 2020;65(7):075003.
- Ahmad SB, Sarfehnia A, Paudel MR, et al. Evaluation of a commercial MRI Linac based Monte Carlo dose calculation algorithm with GEANT 4. Med Phys. 2016;43(2):894-907.
- 22. Kawrakow I, Mainegra-Hing E, Tessier F, Walter BRB. The EGSnrc C++ class library, 2009.
- Woodings SJ, van Asselen B, van Soest TL, et al. Technical note: Consistency of ptw30013 and fc65-g ion chamber magnetic field correction factors. *Medical Physics*. 46(8):3739-3745. https://aapm.onlinelibrary.wiley.com/doi/pdf/10.1002/mp.13623
- Reynolds M, Rathee S, Fallone BG. Ion chamber angular dependence in a magnetic field. Med Phys. 2017;44(8):4322-4328.
- Asselen Bv, Woodings SJ, Hackett SL, et al. A formalism for reference dosimetry in photon beams in the presence of a magnetic field. *Phys Med Biol*. 2018;63(12):125008.

- Pojtinger S, Dohm OS, Thorwarth D. Optimal orientation for ionization chambers in MRGRT reference dosimetry. Curr. Dir. Biomed. Eng. 2017;3(2):273-275.
- Sechopoulos I, Rogers DWO, Bazalova-Carter M, et al. Records: improved reporting of Monte Carlo radiation transport studies: report of the AAPM research committee task group 268. Med Phys. 2018;45(1):e1-e5.
- Bouchard H, Pooter Jd, Bielajew A, Duane S. Reference dosimetry in the presence of magnetic fields: conditions to validate Monte Carlo simulations. *Phys Med Biol*. 2015;60(17):6639.
- Bielajew AF. Electron Transport in E and B Fields, Springer US. 1988:421-434. https://doi.org/10.1007/978-1-4613-1059-4_19

How to cite this article: Alissa M, Zink K, Kapsch R-P, Schoenfeld AA, Frick S, Czarnecki D. Experimental and Monte Carlo-based determination of magnetic field correction factors $k_{B,Q}$ in high-energy photon fields for two ionization chambers. *Med Phys.* 2023;1-12. https://doi.org/10.1002/mp.16345

APPENDIX A: FANO CAVITY TEST

The report AAPM TG-268²⁷ from the American Association of Physicists in Medicine strongly recommends a Fano test for all Monte Carlo studies of detectors with gaseous cavities. In Monte Carlo simulations, the trajectories of charged particles are approximated by condensed history steps, and it is possible that simulation results incorporating magnetic field effects are inaccurate, especially if particles cross boundaries between materials with high and low densities.

In this work, the charged particle transport was tested under Fano conditions as described by Bouchard et al. 28 and Alissa et al. 18 in presence of a magnetic field for all regions i of the two ionization chamber models. To realize the Fano conditions with an external magnetic field, a radiation source was used that distributes electrons in the whole geometry proportional to the density of the material at the current position. In that way, the number of particles n_i emitted in region i depends on the volume and density of the region i, and thus on the mass m_i of region i. Hence, the total number of particles N emitted by the source and the irradiated mass can be described by the following equation.

$$\frac{n_i}{N} = \frac{m_i}{\sum m_i} \tag{A.1}$$

where $\sum m_i$ is the sum over all masses irradiated by the source. The size of the volume of the Fano source was chosen to be large enough to create secondary particle equilibrium in the regions of interest. The electrons are emitted isotropic in all directions and all bremsstrahlung photons were discharged. Furthermore, all materials were replaced by water. In that case, the following

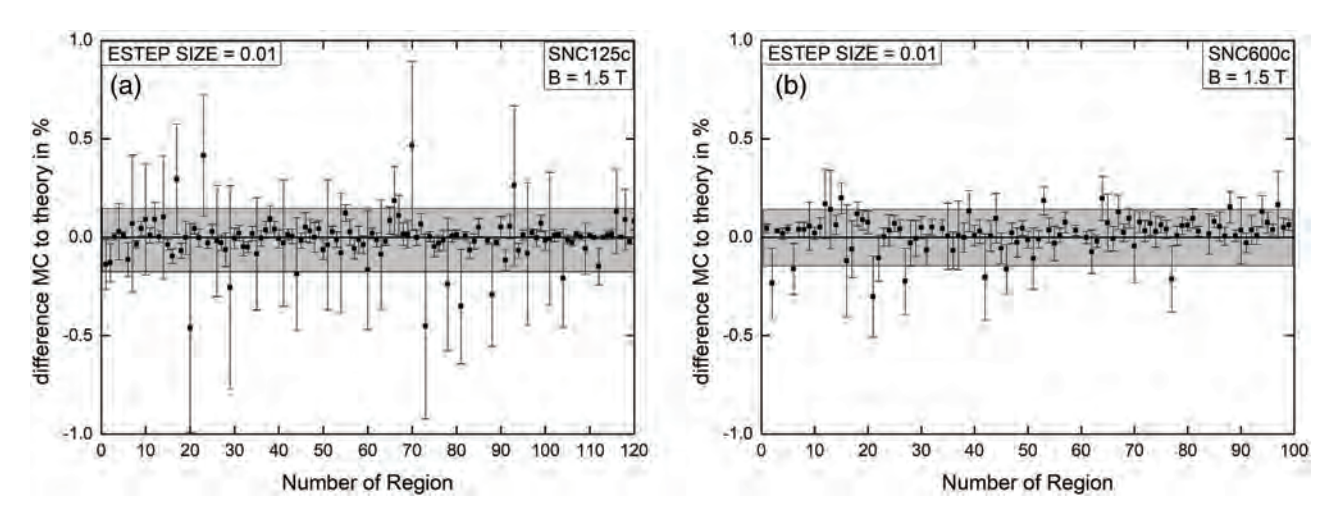


FIGURE A.1 Results of the Fano cavity test for the SNC600c and SNC125c ion chambers in presence of a magnetic field of 1.5 T. The y-axis of both panels show the relative deviation of the Monte Carlo based dose from the expected dose value for each geometrical region of the chambers. The type-A standard uncertainty is represented by the uncertainty bars.

equations holds:

$$D_{\text{MC},i} = n_i \frac{E_0}{m_i} \tag{A.2}$$

where $D_{MC,i}$ is the Monte Carlo-based dose value within the i-th region without normalization to the particle source, E_0 is the energy of the primary electrons of the Fano source, and n_i/m_i is constant for all regions. The Fano particle source included in the EGSnrc c++ class library²² was used and had a volume of 7x5x5 cm³. The energy of the primary electrons was $E_0 = 1$ MeV and the ESTEPE-parameter within the emf_macro.mortran²⁹ was set to 0.01. In addition, all materials of the investigated chambers were replaced by water with the density of the original material. The I-value and the density effect corrections were set to the corresponding values

of water with density $\rho=1$ g/cm³. Monte Carlo results are acceptable, when the relative difference between the theoretically expected value E_0/m_i and the Monte Carlo based dose value $D_{MC,i}$ for every region i within the chamber is less than 0.1%.

The results for the both ion chambers are shown in Figure (A.1). Regarding the small SNC125c chamber, regions 2 and 4 correspond to the active chamber volume and starting from region 10 the volumes belong to the chamber stem. In the SNC600c model, the regions 2 and 6 correspond to the sensitive volume, and the chamber stem regions start with region number 8. Taking into account the uncertainty of the Monte Carlo results, the difference in percent between calculated and expected dose value for all regions of the ionization chambers SNC600c and SNC125c is within 0.1%, i.e. both chambers passed the Fano test for all regions.